Journal of Controlled Release 365 (2024) 274–285

Contents lists available at ScienceDirect

Journal of Controlled Release

journal homepage: www.elsevier.com/locate/jconrel

Co-delivery of drugs by adhesive transdermal patches equipped with dissolving microneedles for the treatment of rheumatoid arthritis

Lijie Zheng [a], Yuanzheng Chen [a,d], Xun Gu [a], Yingying Li [a,b], Hanqing Zhao [a], Wenjun Shao [a], Tao Ma [a,b], Chuanbin Wu [c], Qingqing Wang [a,b,*]

[a] School of Pharmacy, Bengbu Medical College, Bengbu 233030, China
[b] Anhui Engineering Technology Research Center of Biochemical Pharmaceutical, Bengbu Medical College, Bengbu 233030, China
[c] School of Pharmacy, Jinan University, Guangzhou 510006, China
[d] Xiangya School of Pharmaceutical Sciences, Central South University, Changsha 410013, China

ARTICLE INFO

Keywords:
Dissolving microneedles
Adhesive transdermal patch
Rheumatoid arthritis
Complex dosage form
Melittin
Diclofenac sodium

ABSTRACT

In this study, a dosage form consisting of dissolving (D) microneedles (M) and an adhesive (A) transdermal patch (P; DMAP) was designed and pre-clinically evaluated for the treatment of rheumatoid arthritis (RA). The tip of the dissolving microneedles (DMNs) was loaded with the macromolecular drug melittin (Mel@DMNs), this to treat joint inflammation and bone damage, while the adhesive transdermal patches contained the low molecular weight drug diclofenac sodium (DS; DS@AP) for pain relief. Mel@DMNs and DS@AP were ingeniously connected through an isolation layer for compounding Mel-DS@DMAP for the simultaneous delivery of the drugs. *In vitro* and *in vivo* experiments showed that DS@AP did not affect the mechanical properties and dissolution process of Mel@DMNs while the pores formed by the microneedles promoted the skin penetration of DS. Treatment of rats suffering from RA with Mel-DS@DMAP reduced paw swelling and damage of the synovium, joint and cartilage, suggesting that the 'patch-microneedle' dosage form might be promising for the treatment and management of RA.

1. Introduction

Rheumatoid arthritis (RA) is a common, systemic, and chronic autoimmune disease that induces inflammation and resultant pain within the joints. The pathological features linked with this ailment are synovial inflammatory hyperplasia, and cartilage, bone, and joint destruction [1,2]. This typically leads to joint swelling, stiffness, and pain. As the disease advances, it could cause severe joint damage and even disability, significantly affecting human health [3]. Therapeutically treating RA is mainly achieved by administering non-steroidal anti-inflammatory drugs (NSAIDs), glucocorticoids, and disease-modifying antirheumatic drugs [4,5]. NSAIDs are primarily targeted at joint inflammation and pain, and glucocorticoids possess anti-inflammatory and immunosuppressive capacities to treat general inflammatory symptoms [6,7]. Disease-modifying antirheumatic drugs are the preferred treatment for delaying and preventing the progression of RA and joint damage. However, long-term use of disease-modifying anti-rheumatic drugs can lead to toxicity and infections in the gastrointestinal system, skin, kidneys, and other organs [8]. Certain biological macromolecular drugs from natural sources have been shown to significantly reduce RA disease activity and hinder imaging progression [9]. As the unstable structure of biological macromolecules can lead to drug destruction and decomposition by gastrointestinal proteases, injection is the primary method of clinical administration [10]. However, administering through injections demands professional intervention and may lead to complications like bleeding, pain, and infection that could reduce patient compliance, affect efficacy, or even cause treatment discontinuation [11]. Consequently, it is vital to explore alternatives for delivering biological macromolecules that offer the benefits of high bioavailability afforded by injection administration, as well as the convenience, safety, and compliance of oral administration.

Dissolving microneedles (DMNs) are transdermal preparations comprised of water-soluble and biodegradable polymers that possess the aforementioned benefits [12–14]. Furthermore, they are capable of creating temporary micropores in the skin, thus breaching the skin barrier, and directly administering medication to the body, enabling improved topical or systemic administration compared to traditional transdermal delivery [15–17]. In addition, DMNs retain the benefits of

* Corresponding author at: School of Pharmacy, Bengbu Medical College, Bengbu 233030, China.
E-mail address: qingqingwang@bbmc.edu.cn (Q. Wang).

https://doi.org/10.1016/j.jconrel.2023.11.029
Received 7 May 2023; Received in revised form 11 November 2023; Accepted 14 November 2023
Available online 24 November 2023

injectable administration while being painless and facilitating self-administration, leading to improved patient compliance [18,19]. DMNs have been demonstrated significant advantages in delivering biological macromolecules, including insulin [20], vaccines [21], and nucleic acids [22]. Of note, they have been progressively employed in treating RA within the last few years [23–25].

Previously, research has indicated that the use of multiple therapeutic agents concurrently may provide greater efficacy in treating RA compared to using a single treatment option [26–29]. In comparison to general chemical drugs, biological macromolecular drugs exhibit enhanced anti-inflammatory effects, fewer side effects, and prolonged treatment efficacy. Nevertheless, the onset of action is slow, and short-term relief of inflammation and pain in the affected area of the patient is not achievable. Combining NSAIDs can provide short-term symptom relief, making up for the lack of a long-term anti-inflammatory treatment that rapidly relieves joint swelling and pain. NSAIDs are typically taken orally and have anti-inflammatory and analgesic effects [30,31]. However, despite reducing swelling and pain, oral NSAIDs have severe adverse reactions, poor patient tolerance, and minimal treatment effectiveness [32,33]. Research indicates that adhesive transdermal patches (AP) provide local and systemic delivery for NSAIDs. This method bypasses the first-pass effect of the liver, enhancing drug bioavailability [34,35]. Thus, avoiding gastrointestinal and other adverse reactions associated with oral NSAIDs is possible. However, the stratum corneum of the skin creates a barrier that inhibits the transdermal absorption of drugs, resulting in insufficient drug delivery to meet therapeutic requirements. As a result, repeated administration may be necessary [36,37]. Furthermore, the use of multiple formulations for combined administration complicates the treatment process, causing confusion in patients' medication, such as missing or repeated use of a certain drug. This results in the benefits of combined medication not being fully realized.

DMNs and AP are both transdermal delivery formulations and have the basis of combined formulations. If the two are combined into a single formulation, simultaneous multi-drug delivery can be achieved, thereby reducing the number of doses administered and improving patient compliance and therapeutic effect. The needle tips of DMNs are used to load the macromolecular drug, which then dissolves quickly upon insertion into the skin, delivering the drug effectively. AP serves as the underlying layer of DMNs, where the NSAIDs within AP are delivered through the skin to the local tissues for analgesia, while the pressure-sensitive adhesive within it allows DMNs to adhere closely to the skin, enhancing dissolution. Furthermore, the pores formed by DMNs facilitate the delivery of drugs in AP. This co-formulation retains the respective advantages of the two dosage forms, namely DMNs have the dual advantage of transdermal and subcutaneous administration to effectively deliver the drug [38], meanwhile, AP is delivered locally to minimize systemic exposure and thus reduces adverse events [39]. This results in a synergistic and detoxifying dual drug effect achieved with a single administration of the combined formula. However, some issues persist with the preparation method. Firstly, DMNs and AP are combined directly. This can lead to drug diffusion into various parts of the formulation, potentially causing interactions between the two drugs. In addition, the pliable AP is inadequate to provide the required mechanical support for the DMNs array, resulting in the incapacity of DMNs to penetrate the skin. How to overcome these problems and achieve the effect of combined administration and synergistic administration of combined formulation is one of the issues of this study.

Here, we aimed to design a novel composite drug delivery system, named the dissolving microneedles and adhesive transdermal patch (DMAP). Using the anti-inflammatory active macromolecular drug melittin (Mel) as a model drug, the tips of the DMNs, encapsulated in DMAP, were able to deliver Mel effectively *via* the pores created on the skin. This mechanism will improve articular cartilage and reduce synovial damage caused by long-term chronic inflammatory stimulation. Diclofenac sodium (DS), a commonly used nonsteroidal anti-inflammatory drug, is loaded into the AP component of DMAP to achieve rapid pain relief. At the same time, an isolation layer is cleverly added between DMNs and AP, which plays the role of drug isolation during the formulation and storage of DMAP. Furthermore, the isolation layer provides sufficient mechanical support for the DMNs to help penetrate and deliver the drug. Along with percutaneous penetration, DS can also permeate the body through pores created by DMNs, thereby increasing the permeability of AP. This study provides innovative formulations for multi-drug combination therapy for rheumatoid arthritis.

2. Materials and methods

2.1. Materials

Melittin (Mel) was purchased from Shanghai Apeptide Co., Ltd. (Shanghai, China). Diclofenac sodium (DS) was purchased from Aladdin Biochemical Technology Co., Ltd. (Shanghai, China). Polyvinylpyrrolidone (PVP) K90 was obtained from BASF (Ludwigshafen, Germany). Hyaluronic acid (HA) was bought from Huaxi Furuida Biotechnology Co., Ltd. (Jinan, China). All other materials were of reagent grade. ELISA kits for interleukin (IL) -10, IL-1β, and IL-6 were purchased from RayBiotech. (Norcross, GA, USA). ELISA kits for IL-2 and IL-17 were procured from Quanzhou Ruixin Biological Technology Co., Ltd. (Quanzhou, China).

2.2. Animal and cell culture

Male Sprague-Dawley (SD) rats (SPF grade) were purchased from Jinan Pengyue Experimental Animal Breeding Co., Ltd. (Jinan, China) (License no: SCXK(LU)20,190,003). The experimental procedures were carried out in strict accordance with the guidelines for animal experimentation of Bengbu Medical College and were approved by the Institutional Animal Care Committee of the College (Ref. no. 169, 2022).

Rheumatoid arthritis fibroblast-like synoviocytes (RA-FLs) were cultured in Dulbecco's modified Eagle medium supplemented with 10% fetal bovine serum and 1% penicillin/ streptomycin in an incubator at 37 °C under 5% CO_2.

2.3. Fabrication and formulation optimization of DS@AP

2.3.1. Fabrication of the DS@AP

One mL of DS solution (160 mg/mL) was added with transdermal penetration enhancer. Then, add the polyacrylic acid pressure-sensitive adhesive [40] to make the total mass 10 g under stirring. Subsequently, the mixture was vacuumed for 20 min and left to stand overnight. Next, 0.5 mL of the mixture was added to the polydimethylsiloxane (PDMS) mold for drying and molding at a constant temperature. To obtain DS@AP, 33.3% PVP K90 aqueous solution (*w/v*) was added as the base layer and then dried. The morphologies of the prepared DS@AP were observed under a microscope (Leica Camera AG, Wetzlar, Germany).

2.3.2. Formulation optimization of the DS@AP

The TPY-2 Franz diffusion cell device (Shanghai Huanghai Pharmaceutical Inspection Instrument Co., Ltd., Shanghai, China) was utilized to evaluate the permeation characteristics of varied DS@AP formulations, with the aim of optimize the type (azone, isopropyl myristate, propylene glycoland, and oleic acid) and ratio (2%, 5% and 8%) of permeation enhancers. After attaching the different formulations of DS@AP to the skin stratum corneum, they were mounted in combination with a Franz diffusion cell. Samples (0.7 mL) were taken at the pre-set time points of 0.5, 1, 2, 4, 8, 12, and 24 h under the stirring condition of 300 rpm at 32 ± 0.5 °C, and an equal amount of blank phosphate-buffered saline (PBS) was added immediately. The samples were analyzed using high-performance liquid chromatography (SPD-16, Shimadzu, Japan).

2.3.3. In vitro drug release study of the DS@AP

The study of dissolution *in vitro* employed the automatic sampling dissolution apparatus (Liyang Enterprises Co., Ltd., Hong Kong, China) with a speed set to 100 rpm and a dissolution medium of 300 mL PBS. Samples of 0.7 mL were taken at time points of 0.17, 0.5, 1, 2, 4, 8, 12, 24, 36, 48, 60, and 72 h, with an immediate supplement of 0.7 mL of blank PBS. The samples underwent filtration before analyzing and calculating the release degree at each time point using high-performance liquid chromatography. This allowed for the drawing of the release curve. A commonly used mathematical model [41] was used for the curve fitting analysis.

2.4. Fabrication and characterization of Mel@DMNs and Mel-DS@DMAP

A brass mold was manufactured *via* computer-aided design and precision engineering techniques, following which, the negative mold of PDMS was prepared [42]. The mold is divided into three components: the central DMNs region, the isolation layer, and the AP part. 300 mg of HA and 100 mg of Mel solution were added to 1 mL of water and mixed to prepare the needle tip solution of DMNs. An isolation layer solution contained 20% aqueous PVP K90 solution (*w/v*), and a backing layer solution contained 33.3% aqueous PVP K90 solution (w/v).

The DMNs and DMAPs were prepared using a two-step centrifugal needle-making method previously established in the laboratory [43]. The preparation process is shown in Fig. 1: Firstly, approximately 0.12 mL of the needle tip solution was added to the PDMS mold, followed by centrifugation (Thermo Electron LED GmbH, Osterode, Germany), removal of excess solution, and drying for 12 h. Then, 0.1 mL of isolation layer solution was placed above the needle and dried for 12 h. Next, 0.5 mL of AP solution was added and dried for 24 h. Finally, 0.45 mL of the backing layer solution was added, centrifuged, and dried for 1–2 days, and then peeled from the PDMS mold to obtain Mel-DS@DMAP. Subsequently, 0.45 mL of the backing layer solution was added directly onto the surface of the tip layer, and then centrifuged, dried, and de-molded, to obtain Mel@DMNs. DMAP contains only DS (DS@DMAP) was prepared using the same method. (See Scheme 1.)

The morphologies of the prepared Mel@DMNs and Mel-DS@DMAP were observed using a microscope and scanning electron microscope (SEM), and the needle length and drug loading of DMNs were investigated.

2.5. Mechanical properties of the Mel-DS@DMAP needles

The mechanical properties of Mel@DMNs and Mel-DS@DMAP were assessed using a texture analyzer [44] (CT3, Brookfield, USA). The sample tip was positioned upward on the stage of the mass analyzer, with a trigger force of 0.05 N, a loading force of 50 N, and a compression rate of 0.5 mm/s. The needle height was measured under a microscope.

DMAP was prepared by using a 0.4% trypan blue solution instead of water as the needle tip solvent. The cuticle of the skin was placed after epilation upwards, and then DMAP was pressed against the skin for approximately 30 s, then removed after 3 min, and the DMAP-induced penetrations in the skin, to form the pores, were observed.

2.6. In vivo dissolution study of the Mel-DS @DMAP needles

After removing the back hair of the rats, Mel@DMNs and Mel-DS@DMAP were pressed on the skin respectively for a specific duration of time [45](0, 2, 4, 6, 8, 10, 15, 20 min, respectively). At each time point, the sample was taken out and the remaining length of the needle was measured with a microscope. Based on the obtained data, a dissolution trend line was plotted with time as the x-axis and the percentage of remaining needle length as the y-axis.

2.7. In vitro skin permeation of the DS@DMAP

According to the *in vitro* transdermal test method of DS@AP, DS@AP and DS@DMAP were combined with the Franz diffusion cell after attaching them to the stratum corneum, and samples were taken at 0.5, 1, 2, 4, 8, 12, and 24 h after the start of the test and analyzed by high-performance liquid chromatography.

2.8. In vivo analgesic effect of the DS@DMAP

The analgesic effects of DS@AP and DS@DMAP were compared using the hot plate method (YLS-6 A Intelligent Hot Plate Instrument, Shandong Province Academy of Medical Sciences Equipment Station). The experiments were set up in the control group, DS@AP group and DS@DMAP group. Three rats were set up in each group, and each rat was given one tablet of the formulation transdermally in the leg, and the rats were placed individually on the hot plate (52 ± 0.5 °C) after 8 h of administration. When the rats showed the first licking of the hindfoot, the heating was stopped immediately and the timepoint was recorded.

2.9. Cytotoxicity

RA-FLs were seeded into a 96-well plate with a density of 5×10^3 cells per well. The concentration of the drug in the Mel group, the DS group, as well as in the combined Mel and DS group was fixed at 5–100 μg/mL. 20 μL of 3-(4,5-dimethylthiazol-2-yl)-2,5-diphenyl tetrazolium bromide (MTT) (5 mg/mL) was added after 24 h, the supernatant was discarded after 4 h of incubation, and the pellet was dissolved in 150 μL of dimethyl sulfoxide. The absorbance of the resulting solution was measured.

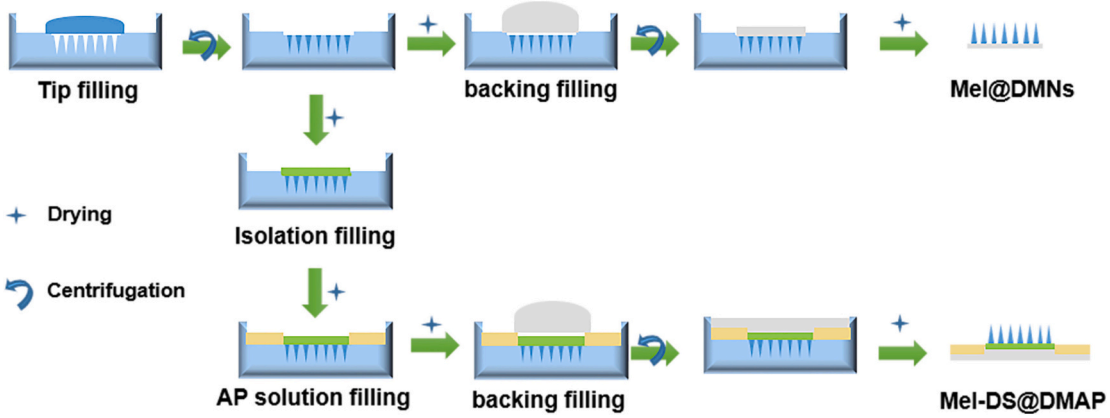

Fig. 1. Fabrication principle of Mel@DMNs and Mel-DS@DMAP.

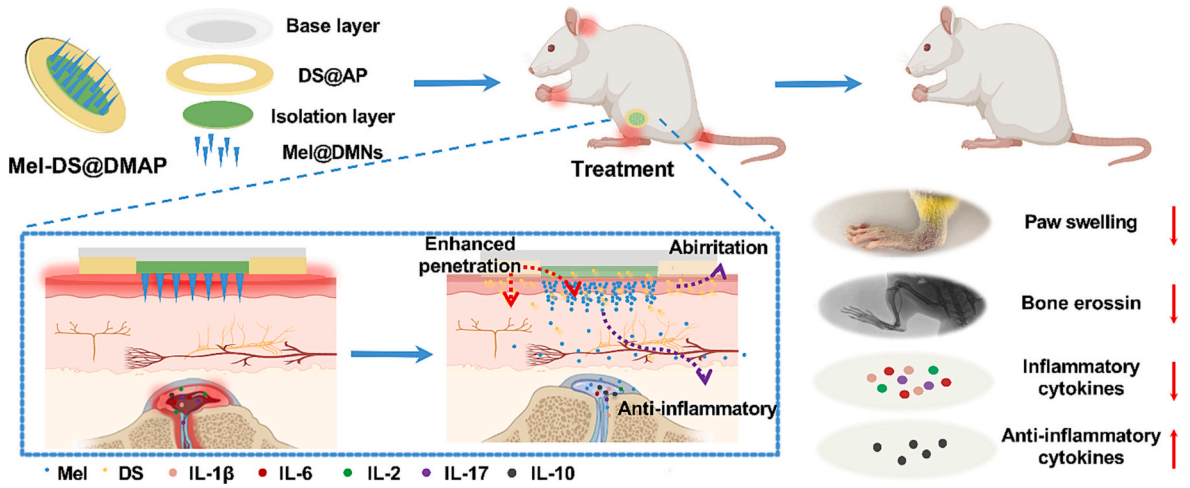

Scheme 1. A new complex dosage form consisting of dissolving microneedles and adhesive transdermal patch (DMAP) has been designed and prepared by a simple and effective method for the treatment of rheumatoid arthritis. Mel-DS@DMAP: DMAP containing melittin and diclofenac sodium, DS@AP: adhesive transdermal patch containing diclofenac sodium, Mel@DMNs: dissolving microneedles containing melittin.

2.10. Pharmacodynamics studies

2.10.1. Establishment and treatment of AA rat model

The purpose of this experiment was to investigate the pharmacodynamics of Mel-DS@DMAP in AA rats. An injection was subcutaneously administered to the rat's disinfected right hind foot. The Normal group was given an injection of 0.1 mL of normal saline, while the other modeling groups were given an injection of 0.1 mL of complete Freund's adjuvant (CFA) to create an AA rat model [46]. To determine the success of the model, we analyzed the level of redness and swelling in the rat joints, as well as swelling and deformation.

Four groups of AA rats, ($n = 5$), were randomly allocated to the Model group, DS@AP group, Mel@DMNs group, and Mel-DS@DMAP group. Treatment was initiated on day 18. The drug was administered once every 3 days for a total of 21 days.

2.10.2. Swelling of rat paw

The volume of secondary claws of rats in each group was measured using a paw volumeter (Anhui Zhenghua Biotechnology Co., Ltd., Anhui, China) every three days before (V0) and after (Vt) modeling. The following formulas were used to evaluate the paw swelling rate before treatment and the paw swelling degree after treatment:

$$\text{Paw swelling rate } (\%) = \mathrm{Vt}/\mathrm{V_0} \times 100$$

$$\text{Degree of paw swelling } (\%) = (\mathrm{Vt} - \mathrm{V_{18}})/\mathrm{V_{18}} \times 100$$

2.10.3. Radiological examination

To assess the degree of joint damage in each group following treatment, all groups of rats underwent X-ray imaging (Bruker *in vivo* Multispectral FX PRO, USA) of their left ankle and hindlimb after the final dose on day 39.

2.10.4. Histological analysis of synovium and ankle joint

Rats were sacrificed after the treatment, and the synovium and ankle joint of the left leg were removed. The synovial tissue was paraffin-embedded and sectioned, and the ankle joint was decalcified and paraffin-embedded before sectioning. The sections were stained with Hematoxylin-Eosin (H&E) and Saffron O/Fast Green, and the staining results were observed under a microscope.

2.10.5. Serum cytokine detection

After the treatment, venous blood was collected from the rats' orbits, left to stand for 4 h, and then centrifuged at a speed of 5000 rpm for 15 min to obtain serum. The serum levels of cytokines, including IL-2, IL-6, IL-1β, IL-17, and IL-10, were determined using rat ELISA kits [46].

2.11. Statistical analysis

The experimental data are expressed as the mean ± standard deviation, and the data analysis and processing are completed by SPSS 21.0.0.0, GraphPad Prism 8.01, and other software. *t*-test and one-way ANOVA were used to evaluate the difference in the data. The statistical significance was set as $P < 0.05$.

3. Results

3.1. Fabrication and characterization of DS@AP

3.1.1. Formulation optimization of DS@AP

Incorporation of a transdermal penetration enhancer into the AP formulation can substantially enhance the effectiveness of the AP by facilitating drug penetration through the skin. DS@AP was prepared with varying penetration enhancers, and the impact of different formulations on skin permeability was investigated using a Franz diffusion cell (Fig. 2A-B). The types and contents of transdermal penetration enhancers were screened and optimized by taking the drug transdermal penetration rate as the index. First, a fixed content of 5% was initially used, and one out of the four enhancers was chosen as the optimal choice (refer to Fig. 2C). Where Js represents the slope of the 0–24 h curve, indicating the average rate of drug permeation, while Qn signifies the cumulative permeation within 24 h, per unit area. In comparison to the control group, both the azone group and the isopropyl myristate group showed similar and smaller Js values. Furthermore, neither the azone nor the isopropyl myristate group demonstrated a noticeable increase in drug permeability. The Js and Qn values of the propylene glycol and oleic acid groups were significantly higher than those of the control group, wh ich demonstrated a superior penetration effect for the propylene glycol group. As a result, propylene glycol was selected as the optimal transdermal penetration enhancer.

The optimal content for the preferred penetration enhancer was determined by testing three mass fractions of 2%, 5%, and 8% (refer to Fig. 2D). Compared to the control group, the propylene glycol group with varying concentrations exhibited higher Js and Qn values. Among them, the 5% propylene glycol group exhibited superior penetration-promoting effects. Consequently, 5% propylene glycol was identified as the final penetration-promoting agent.

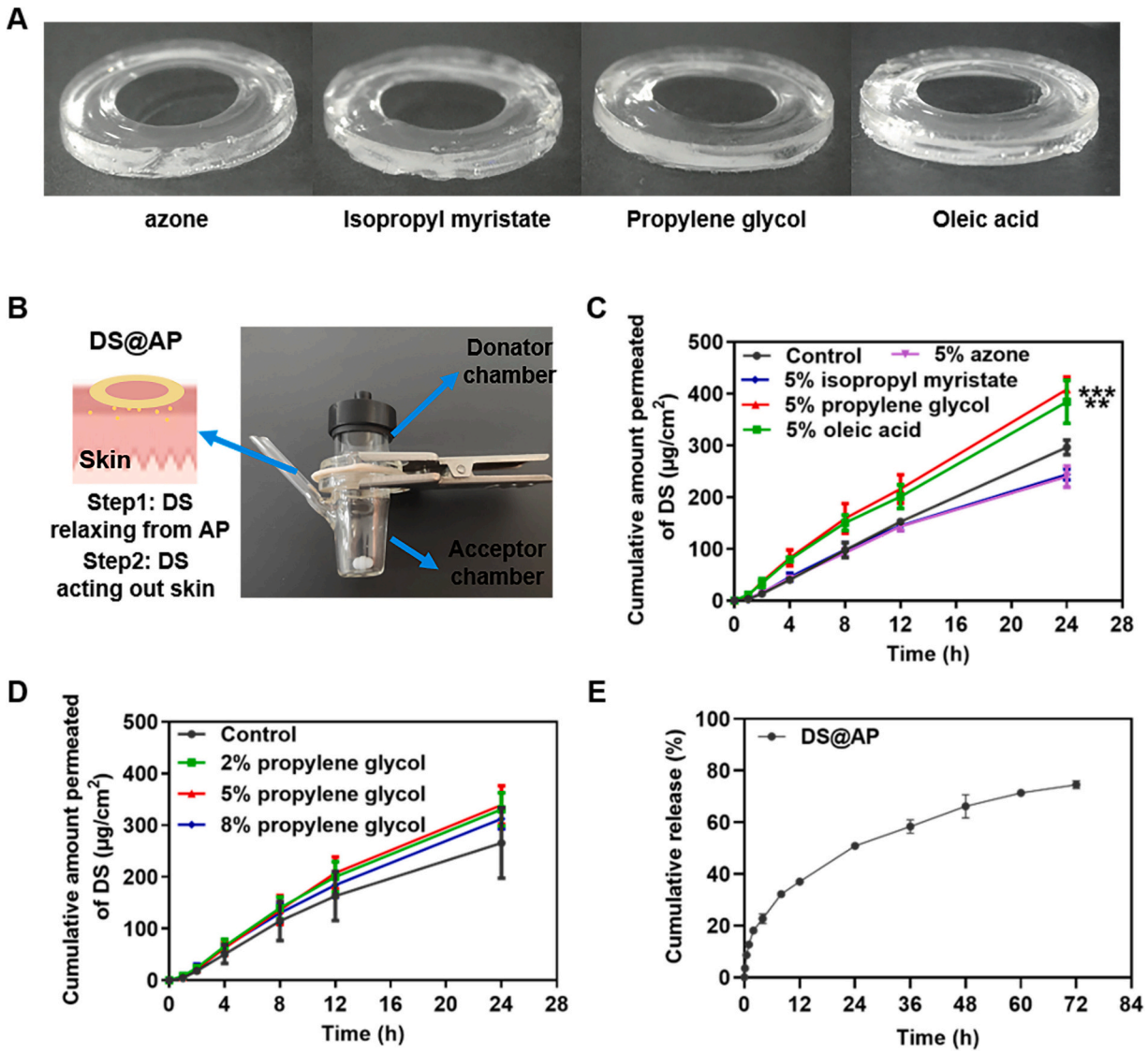

Fig. 2. Characterization and analysis of the *in vitro* permeation behavior of different AP formulations. (A) DS@AP graphics with different penetration enhancers (Azone, Isopropyl myristate, Propylene glycol, Oleic acid); (B) A diagram of the screening device for penetration enhancer and its effects on the skin. *In vitro* skin permeation curves of DS@AP (C) with different kinds of penetration enhancers (D) with different contents of propylene glycol. ($\bar{x} \pm s$, $n = 3$), with the control group, $^{**}P < 0.01$, $^{***}P < 0.001$. (E) Drug release behavior of DS@AP containing 5% propylene glycol. ($\bar{x} \pm s$, $n = 3$).

3.1.2. Drug release study of the DS@AP

In Vitro drug release from DS@AP is shown in Fig. 2E. Drug release in AP increased over time, particularly in the first 2 h, leading to the release of 18.12% of the drug. The release rate increased to 75% over 72 h. To investigate the release mechanism of the drug from the patch, the drug release curve was fitted to the Ritger-Peppas mathematical model, and a judgment on the release mechanism was made based on the fitted results. The fitting equation: $y = 13.29t^{0.41}$, $R^2 = 0.99645$, in which the dissolution characteristic the index $n = 0.41$ (< 0.45), characterizing dissolution points to conformity with Fick's first diffusion law.

3.2. Fabrication and characterization of Mel@DMNs and Mel-DS@DMAP

Mel@DMNs, DS@AP, and Mel-DS@DMAP were prepared respectively (Fig. 3A-C). The images indicate that DMNs and AP combine to form a novel complex dosage, which resembles a regular torus that measures 2 cm in outer diameter and 1 cm in inner diameter. The outer ring section comprises DS@AP, which is transparent and colorless, with an area of approximately 2.355 cm^2. The amount of DS content is 8.20 ± 0.078 mg (Fig. S1). The central core comprises of Mel@DMNs, with 89 well-arranged and smooth conical needles measuring 792.92 ± 12.89 μm in height (Fig. 3D). Furthermore, the Mel content of 110.00 ± 10.00 μg, and the drug content was stable after 8 weeks of storage under dry conditions (Fig. S2A).

3.3. Isolation layer

DMNs and AP are connected by the isolation layer and combined into a whole (Fig. 3G), rhodamine B (Rh—B) was substituted for DS to prepare DMAP without the isolation layer (Fig. 3E) and DMAP with the isolation layer (Fig. 3F). The DMAP needle with the presence of the isolation layer becomes transparent, preventing the permeation of red Rh—B, in contrast to DMAP without an isolation layer. It shows that the isolation layer plays the role of connecting different formulations and isolating drugs, therefore avoiding drug interactions that may affect efficacy.

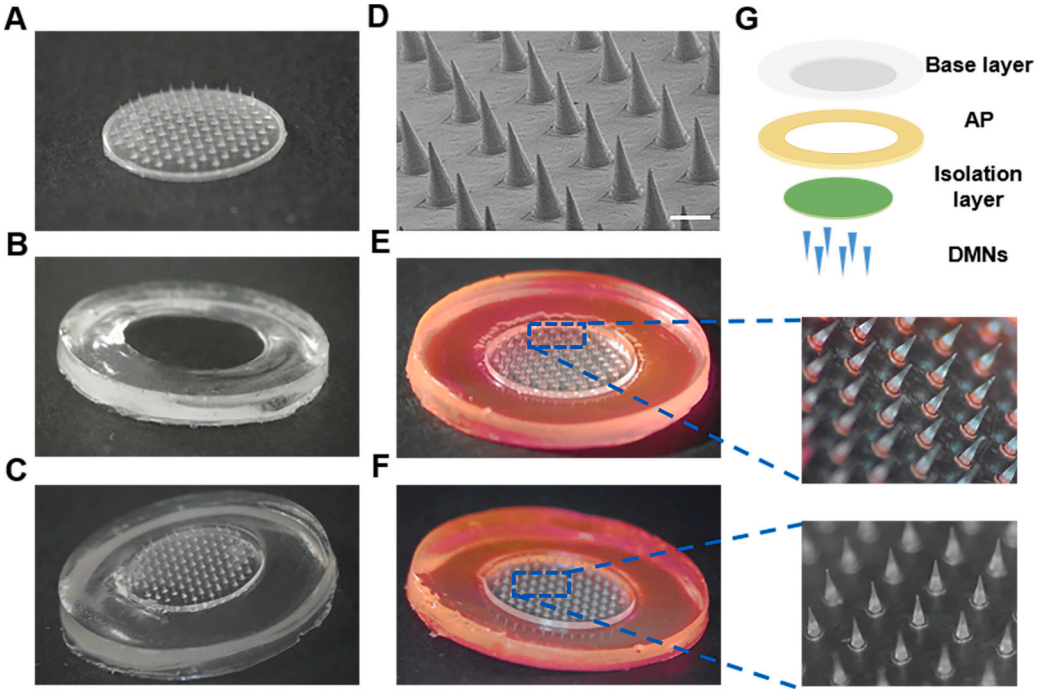

Fig. 3. Characterization of DMAP and its parts. (A) Microscope image of the Mel@DMNs, (B) DS@AP and Mel-DS@DMAP (C). (D) SEM image of the Mel@DMNs, scale bar: 400 μm. Mel-Rh-B@DMAP without (E)/with (F) isolation layer. (G) Exploded view of the components of DMAP.

3.4. The effect of AP on DMAP

3.4.1. Mechanical properties of Mel-DS@DMAP

The changes in needle length post-compression of Mel@DMNs and Mel-DS@DMAP were drecorded through microscope examination (Fig. 4A). The height of Mel@DMNs and Mel-DS@DMAP both decreased by 17.45% and 17.65%, correspondingly. The difference was not statistically substantial, indicating that the two formulations have similar mechanical properties. Mel-DS@DMAP remains mechanically stable post an 8-week storage duration (Fig. S2B).

The results of the *in vitro* skin insertion test for Mel@DMNs and Mel-DS@DMAP are shown in Fig. 4B-C. Both formulations could penetrate the stratum corneum completely with a 100% piercing rate. These findings indicated that the integration of AP and DMNs into DMAP does not affect the ability of DMAP to penetrate the stratum corneum.

3.4.2. Study on the dissolution of Mel-DS@DMAP in vivo

The images of needle length change for Mel@DMNs and Mel-DS@DMAP formulations revealed comparable needle dissolution (Fig. 4D-E). Complete dissolution of both types of needles occurred within 20 min. Microscope images were consistent with needle length measurements (Fig. 4F), and there was no significant difference between the two formulations. This suggested that AP did not impact the dissolution of DMNs within skin tissue after binding DMNs to AP. It was found that the Mel-DS@DMAP needles dissolved more within 20 min. This was likely attributed to the viscosity of AP, which facilitated a close fit of the DMNs with the skin, thereby enhancing the dissolution of the DMNs. We could conclude that the initial rapid and subsequent slow dissolution profile of DMNs could be attributed to the gradual increase in volume and cross-sectional area of the needle body from tip to toe in the direction of the needle. This resulted in an increase in resistance during the insertion process of DMNs. At the same time, the dissolution process is influenced by the elasticity of the skin tissue, the material and geometry of the DMNs, and the limited local skin tissue fluid.

3.4.3. Inhibitory effects of combined drugs on inflammatory cells in vitro

The effects of different drugs on the survival of RA-FLs were studied using the MTT assay (Fig. 4G). DS displayed a negligible effect on cell viability at the concentration of 5–100 μg/mL. Nevertheless, cell viability obviously decreased with the increased concentration of Mel. Furthermore, simultaneous administration of Mel and DS demonstrated higher cytotoxicity than Mel alone. These results indicated that Mel played a major role in inhibiting the proliferation of RA-FLs, and the combined administration of Mel and DS has a better effect on inhibiting the proliferation of RA-FLs.

3.5. The effect of DMNs on drug release in AP

Whether DMNs affect drug release in AP was investigated by comparing the transdermal penetration effect of the two formulations. It was found that the DS@DMAP group had a faster penetration rate than the DS@AP group (Fig. 5A). Besides, the cumulative penetration level of the DS@DMAP group was significantly higher than that of the DS@AP group. The above results indicated that the transdermal effect of DS@DMAP was significantly higher than that of the DS@AP group, and indicated that DMNs in the combined formulation had a promoting effect on drug release in AP.

The two DS formulations were applied to the skin of rats (Fig. 5C-D), to explore the analgesic effect *in vivo*. The pain thresholds of the rats in the DS@AP group and the DS@DMAP group were found to be higher compared to the control group, suggesting that both DS formulations produced analgesic effects on the rats (Fig. 5B). Although there was no significant variance in pain threshold between the DS@AP group and the control group, there was a notable difference between the DS@DMAP group and the control group. Moreover, the dosage of DMAP and AP delivered DS was 1.62 0.1 mg/kg and 1.51 0.1 mg/kg, respectively (Fig. S3). This indicates that the DS@DMAP group works better, which is supported by the transdermal penetration results in Fig. 5A.

The combination of DMNs and AP did not reduce percutaneous drug penetration in AP, but instead increased the drug release rate and improved the analgesic effect. The reason may be that the presence of DMNs and the resulting pores facilitated rapid drug delivery. Moreover, the drug in AP not only directly penetrated the skin, but also spread to the DMNs area *via* the softened isolation layer before entering the skin

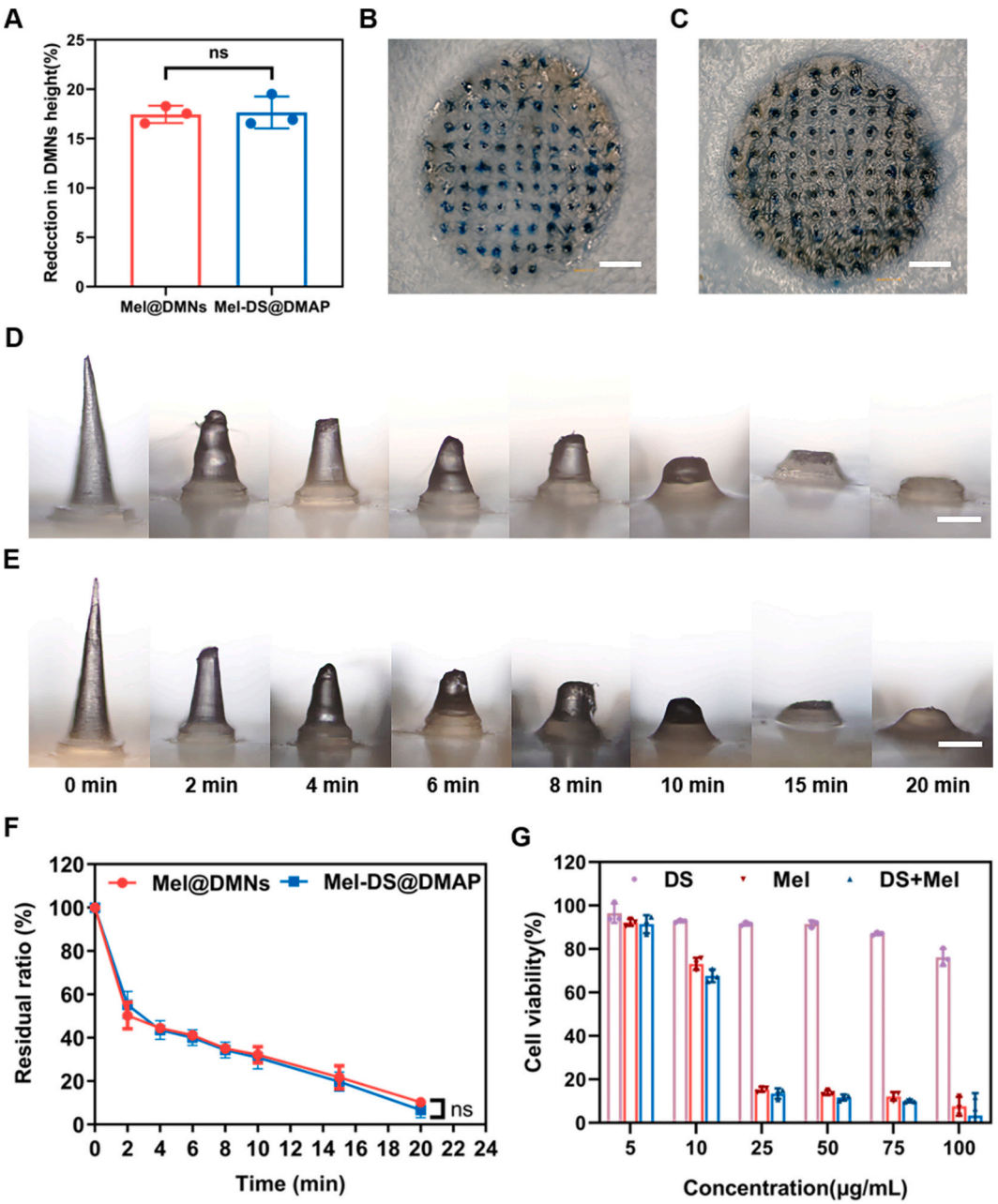

Fig. 4. *In vitro* and *in vivo* experiments of Mel@DMNs and Mel-DS@DMAP. (A) Percent reduction in height of Mel@DMNs and Mel-DS@DMAP needles after compression using the texture analyzer compared with that before compression. ($\bar{x} \pm s$, $n = 3$). (B-C) Results of *in vitro* rat skin insertion studies using Mel@DMNs and Mel-DS@DMAP, scale bar: 2 mm. Needles dissolution images of (D)Mel@DMNs and (E)Mel-DS@DMAP inserted into the skin of living rats at different times. Scale bar: 200 μm. (F) Percentage curves of remaining length of needle after dissolution at different time points of Mel@DMNs and Mel-DS@DMAP. ($\bar{x} \pm s$, $n = 5$). (G) *In vitro* inhibitory effect of DS, Mel, DS and Mel on RA-FLs. ($\bar{x} \pm s$, $n = 3$).

through the micropores.

3.6. Pharmacodynamics studies

3.6.1. Swelling of rat paw

The establishment of the AA rat model and the schematic diagram of the treatment plan are shown in Fig. 6A. AA rats have demonstrated significant weight fluctuations, which may be attributed to the disease (Fig. S4). To establish and treat arthritis models, the degree of secondary paw swelling in rats was measured as a direct marker. The results demonstrated that the secondary paw of rats showed signs of swelling on the 12th day following CFA induction and that this swelling significantly increased on the 18th day. There were significant differences between each group and the Model group ($P < 0.001$, Fig. 6B); indicative of the successful induction of the AA rat model. Paw swelling of rats in each group varied throughout treatment, with the highest level of swelling occurring on the 21st day (Fig. 6C). The paw swelling decreased on the 21st day because of the autoimmune and therapeutic effects. After the treatment, the paw swelling increased by 1.52% and 0.97% in the Model group and the DS@AP group respectively. Mel@DMNs and Mel-DS@DMAP showed decreased paw swelling by 18.92% and 11.71% respectively. It could be found that the paw swelling in the Mel-DS@DMAP group was significantly reduced compared with that in the Model group ($P < 0.01$), indicating the superior efficacy of Mel-DS@DMAP in relieving paw swelling.

The condition of the secondary paws was observed post-treatment

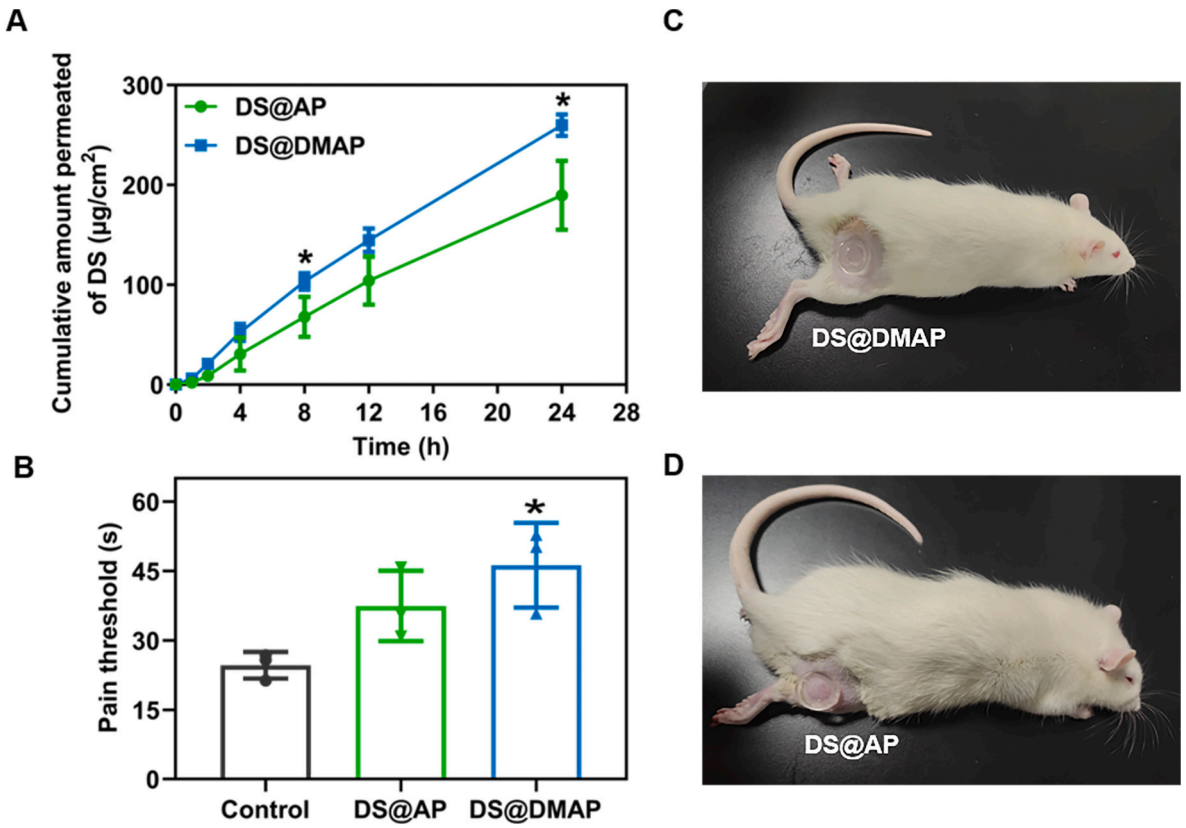

Fig. 5. Analgesic effect of DS@DMAP *in vitro* and *in vivo*. (A) Cumulative infiltration per unit area of DS@AP and DS@DMAP within 24 h ($\bar{x} \pm s$, $n = 3$), compared with DS@AP group, $^*P < 0.05$. (B) Effects of DS@AP and DS@DMAP on pain threshold in rats ($\bar{x} \pm s$, $n = 3$), compared with the control group, $^*P < 0.05$. (C) DS@DMAP and DS@AP (D) were applied to rat skin.

(Fig. 6D). Evidently, the paws of Model group rats were significantly swollen compared to the Normal group. The treated groups exhibited varying degrees of alleviation in swelling. In contrast, the outcomes of the Mel-DS@DMAP group resembled those of the Normal group. These results demonstrate the efficacy of Mel-DS@DMAP in reducing paw swelling in AA rats.

3.6.2. Radiological examination

Radiographic examinations were conducted on every group (Fig. 6E). The Model group exhibited significant soft tissue swelling, reduced local bone density, and a presence of bone defect compared to the Normal group. Furthermore, the secondary paw swelling in the other treatment groups was significantly improved when compared to the Model group. Among them, the rats in the Mel@DMNs and Mel-DS@DMAP groups had results closer to those of the Normal group. This was indicated by lower paw swelling, higher bone density, and fewer bone defects. It can be inferred that both of these groups are effective in reducing secondary paw swelling, surpassing the outcomes observed in the other groups. This suggests that that Mel has a significant impact on reducing both paw swelling and bone damage.

3.6.3. Histological analysis of synovium and ankle joint

To verify the therapeutic effect of Mel-DS@DMAP, the synovial tissue was analyzed by H&E staining (Fig. 7A). The synovial tissue of the Model group exhibited abnormal proliferation, coupled with infiltration of inflammatory cells and formation of pannus. However, the histopathological changes of each treatment group were slightly mitigated to an extent. The pathological condition of the Mel@DMNs and Mel-DS@DMAP groups resembled that of the Normal group, displaying superior therapeutic outcomes compared to other treatment groups.

An H&E staining of the ankle joint revealed that the articular surface of the Normal group's articular cartilage was smooth with no presence of inflammatory cell infiltration. In contrast, the untreated Model group showed significant shedding and inflammatory cell infiltration on their articular surface. Notably, the treatment group's overall condition improved. Specifically, the joint surfaces of the Mel-DS@DMAP groups closely resembled those of the Normal group, presenting flat articular surfaces (Fig. 7B). Similarly, the staining of ankle joints using Saffron O/fast green revealed a darker stain in the Normal group, while the Model group had joint degeneration and a lighter stain. In comparison, the staining in the DS@AP group, Mel@DMNs group, and Mel-DS@DMAP group gradually became darker than the Model group (Fig. 7C).

Based on the findings from the synovial and ankle staining analysis above, it has been established that the Mel-DS@DMAP group had an optimal effect in reducing synovial inflammation and joint damage in AA rats.

3.6.4. Serum cytokine detection

Cytokines have a crucial function in the regulation of the body's immune and inflammatory responses and are significant factors in synovial inflammation development, articular cartilage, and bone destruction. Therefore, this study explored different formulations' role in regulating cytokine balance by measuring serum levels of pro-inflammatory cytokines (IL-2, IL-6, IL-1β, IL-17) and anti-inflammatory cytokine IL-10 in AA rats.

As shown in Fig. 8, there was a significant increase ($P < 0.05$) in the levels of pro-inflammatory cytokines IL-2, IL-6, IL-1β, and IL-17 in the serum of AA rats induced by CFA when compared to the Normal group. Additionally, there was a significant decrease ($P < 0.001$) in the expression of the anti-inflammatory cytokine IL-10. These results suggested that the development of RA disease is associated with an increase in inflammatory cytokines and a reduction of anti-inflammatory

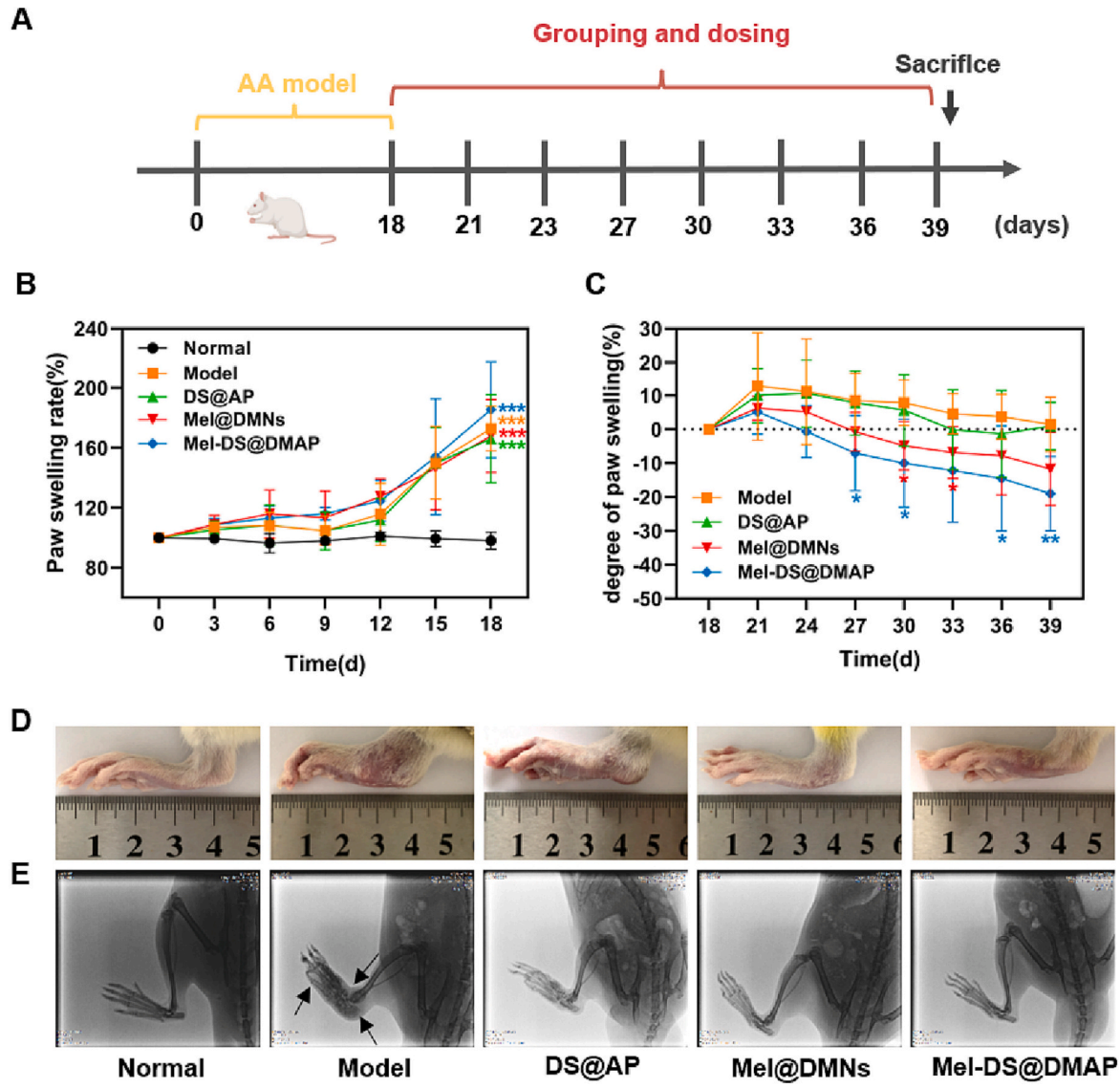

Fig. 6. AA rat model establish and treatment. (A) AA rat model erection and treatment plan. (B) Change in paw swelling rate of rats during model establishment. It can be inferred that the paw swelling rate was 100% before modeling. ($\bar{x} \pm s$, $n = 5$). ***$P < 0.001$ compared with the Normal group. (C) Change in degree of paw swelling of development of AA rats in the course of treatment, compared with the 18th day. ($\bar{x} \pm s$, n = 5). *$P < 0.05$, **$P < 0.01$, when compared with the Model group. (D) Secondary side paws swelling of rats in different groups on the 39th day. (E) Radiological study of secondary side paws in rats in the different groups on the 39th day.

cytokines. Following treatment, inflammatory cytokines were down-regulated to differing extents. Notably, only the levels of IL-6 and IL-17 decreased significantly in the DS@AP group, whereas four inflammatory cytokines exhibited significant reductions in Mel@DMNs and the Mel-DS@DMAP groups (Fig. 8A-D). The expression level of the anti-inflammatory cytokine IL-10 increased to varying degrees in each treatment group (Fig. 8E). Notably, the Mel@DMNs group showed a slight increase in IL-10 levels, whereas the DS@AP group had an obviously elevated serum IL-10 level ($P < 0.01$). Moreover, the Mel-DS@DMAP group also significantly increased the serum IL-10 level ($P < 0.05$). Thus, it can be inferred that DS plays a crucial role in up-regulating IL-10.

The results of this experiment presented convincing support that Mel-DS@DMAP could effectively exploit the benefits of administering both Mel and DS simultaneously. As a result, there was a marked regulation of the balance between pro-inflammatory and anti-inflammatory cytokines in AA rats, leading to a decrease in the systemic inflammatory response. Therefore, this intervention significantly contributes towards mitigating damage to the articular cartilage and bone. After the treatment, its safety could be revealed through further examination of H&E pathological sections of the skin's surface and skin, as well as the H&E pathological observation test of the main organs. As shown in Fig. S5, the two PVP preparations containing DMNs have no obvious allergic reactions on the skin, and there was no noticeable polymer accumulation in skin tissue. The main organs of AA rats in all groups exhibited damage (Fig. S6). Among them, Mel-DS@DMAP had less damage and good biocompatibility.

4. Conclusion

Microneedles, as a new type of drug delivery vehicle, have received widespread attention due to their delivery efficiency and ease of preparation. Nevertheless, there remain several issues that must be resolved before DMAP can be adopted as a practical drug delivery method. Firstly, the preparation process needs to be further improved to enhance safety. The risk of infection is taken into account in the development of

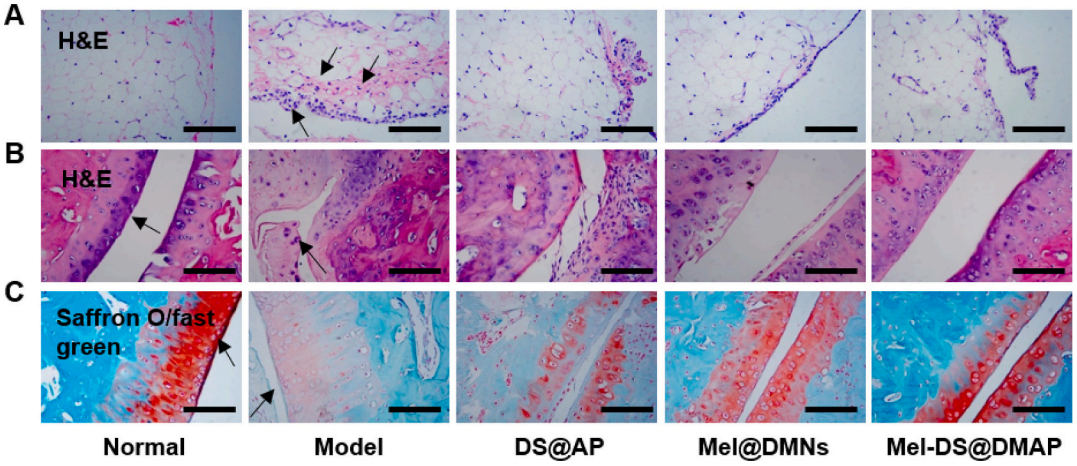

Fig. 7. Histopathological analysis of AA rats treated with different formulations. Synovial tissue H&E staining (A), ankle tissue H&E staining (B) and Saffron O/fast green staining (C) assess histopathological changes, scale: 50 μm. (For interpretation of the references to colour in this figure legend, the reader is referred to the web version of this article.)

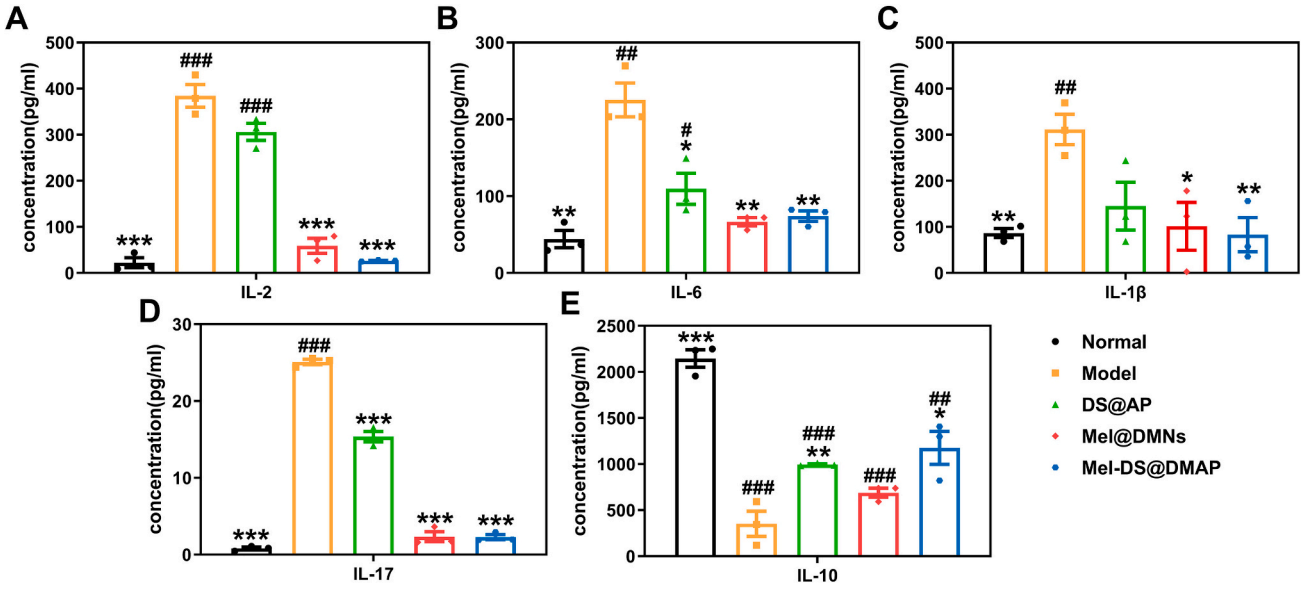

Fig. 8. After the treatment, the serum levels of IL-2, IL-6, IL-1β, IL-17 and IL-10 of rats in each group were determined by Elisa kit. $^{###}P < 0.001$, $^{##}P < 0.01$ *vs* Normal group; $^{***}P < 0.001$, $^{**}P < 0.01$, $^{*}P < 0.05$ *vs* Model group ($\bar{x} \pm s$, $n = 3$).

DMNs products. Currently, DMNs products are considered to be safe and effective for patients if they are sterile or have a low bioburden in specific cases [47]. Secondly, the design of DMNs should consider the efficiency of drug delivery and patient acceptability The longer the tip length, the more efficient the drug delivery, but the stronger the risk of pain and infection. In addition, by increasing the density tip of the DMNs to load enough drug, the number of administrations can be reduced, thereby improving patient compliance. Thirdly, different parts of the body have different stratum corneum thicknesses, densities of skin appendages, and different skin permeability [48]. In our design, considering that the site of administration of RA is usually chosen to be close to the joint lesion, the adhesion of AP to the skin can be improved by making AP thinner and increasing its elasticity, which can be better adapted to the joint area.

In this study, a combined transdermal formulation termed Mel-DS@DMAP, was developed to deliver multiple drugs simultaneously for the treatment of RA. Mel is loaded into the tip of the DMNs to alleviate inflammation and mitigate bone damage, and DS is loaded into AP to alleviate pain. A cleverly inserted isolation layer acts as a means of both support and insulation. Both the *in vitro* penetration experiments and the *in vivo* dissolution experiments have confirmed that the combination of DMNs and AP has a synergistic effect. More precisely, DMNs' pores encourage drug penetration within AP, while AP's adhesion to the skin promotes the dissolution and discharge of drugs from DMNs. *In vivo* pharmacodynamic studies discovered that the joint swelling of rats significantly improved after Mel-DS@DMAP treatment, and the balance of pro-inflammatory and anti-inflammatory cytokines was regulated, thus hindering the progression of RA significantly. Therefore, the new dosage forms DMAP hold great promise as an effective RA treatment strategy, it laid a foundation for the implementation of multi-drug synergistic treatments and provided insights for the treatment of other diseases.

Funding

This research was funded by the Key Projects of Outstanding Young Talents Support Program in the Universities of Anhui Province, grant number gxyqZD2020026, Anhui Provincial Natural Science Foundation,

grant number 2108085MH317, Anhui Province Postdoctoral Researcher Research Activities Funding Project, grant number 2022B626, and Bengbu Medial College Students' Innovation and Entrepreneurship Training Program Project, grant number bydc2022065.

CRediT authorship contribution statement

Lijie Zheng: Writing – original draft, Conceptualization. **Yuanzheng Chen:** Methodology. **Xun Gu:** Validation. **Yingying Li:** Software. **Hanqing Zhao:** Formal analysis. **Wenjun Shao:** Investigation. **Tao Ma:** Visualization. **Chuanbin Wu:** Visualization. **Qingqing Wang:** Writing – review & editing, Resources, Conceptualization.

Declaration of Competing Interest

The authors declare no conflict of interest.

Data availability

Data will be made available on request.

Appendix A. Supplementary data

Supplementary data to this article can be found online at https://doi.org/10.1016/j.jconrel.2023.11.029.

References

[1] Y. Yang, L. Guo, Z. Wang, P. Liu, X. Liu, J. Ding, W. Zhou, Targeted silver nanoparticles for rheumatoid arthritis therapy via macrophage apoptosis and Re-polarization, Biomaterials 264 (2021), 120390.
[2] I.B. McInnes, G. Schett, The pathogenesis of rheumatoid arthritis, N. Engl. J. Med. 365 (23) (2011) 2205–2219.
[3] C.S. Pirmardvand, J. Varshosaz, S. Taymouri, Recent approaches for targeted drug delivery in rheumatoid arthritis diagnosis and treatment, Artif. Cells Nanomed. Biotechnol. 46 (sup2) (2018) 502–514.
[4] S. Zhou, H. Zou, G. Chen, G. Huang, Synthesis and biological activities of chemical drugs for the treatment of rheumatoid arthritis, Top. Curr. Chem. 377 (5) (2019) 28.
[5] S.D. Reichardt, A. Amouret, C. Muzzi, S. Vettorazzi, J.P. Tuckermann, F. Luhder, H. M. Reichardt, The role of glucocorticoids in inflammatory diseases, Cells Basel 10 (11) (2021) 2921.
[6] M. Oray, K. Abu Samra, N. Ebrahimiadib, H. Meese, C.S. Foster, Long-term side effects of glucocorticoids, Expert Opin. Drug Saf. 15 (4) (2016) 457–465.
[7] G. García-Rayado, M. Navarro, A. Lanas, NSAID induced gastrointestinal damage and designing GI-sparing NSAIDs, Expert. Rev. Clin. Pharmacol. 11 (10) (2018) 1031–1043.
[8] R.A. Oliveira, I.M. Fierro, New strategies for patenting biological medicines used in rheumatoid arthritis treatment, Expert Opin. Ther. Pat. 28 (8) (2018) 635–646.
[9] S.T. Law, P.C. Taylor, Role of biological agents in treatment of rheumatoid arthritis, Pharmacol. Res. 150 (2019), 104497.
[10] J. Li, T. Ke, C. He, W. Cao, M. Wei, L. Zhang, J. Zhang, W. Wang, J. Ma, Z. Wang, Z. Shao, The anti-arthritic effects of synthetic melittin on the complete Freund's adjuvant-induced rheumatoid arthritis model in rats, Am. J. Chin. Med. 38 (06) (2012) 1039–1049.
[11] A. Szeremeta, A. Jura-Półtorak, A. Zoń-Giebel, M. Kopeć-Mędrek, E.J. Kucharz, K. Olczyk, Aggrecan turnover in women with rheumatoid arthritis treated with TNF-α inhibitors, J. Clin. Med. 9 (5) (2020) 1377.
[12] D. Khan, M. Qindeel, N. Ahmed, A.U. Khan, S. Khan, A.U. Rehman, Development of novel pH-sensitive nanoparticle-based transdermal patch for management of rheumatoid arthritis, Nanomedicine UK 15 (6) (2020) 603–624.
[13] X. Chen, L. Wang, H. Yu, C. Li, J. Feng, F. Haq, A. Khan, R.U. Khan, Preparation, properties and challenges of the microneedles-based insulin delivery system, J. Control. Release 288 (2018) 173–188.
[14] Y. Hao, W. Li, X. Zhou, F. Yang, Z. Qian, Microneedles-based transdermal drug delivery systems: a review, J. Biomed. Nanotechnol. 13 (12) (2017) 1581–1597.
[15] W. Zhao, L. Zheng, J. Yang, Z. Ma, X. Tao, Q. Wang, Dissolving microneedle patch-assisted transdermal delivery of methotrexate improve the therapeutic efficacy of rheumatoid arthritis, Drug Deliv. 30 (1) (2023) 121–132.
[16] G. He, Y. Li, M.R. Younis, L.H. Fu, T. He, S. Lei, J. Lin, P. Huang, Synthetic biology-instructed transdermal microneedle patch for traceable photodynamic therapy, Nat. Commun. 13 (1) (2022) 6238.
[17] X. Zhang, X. Fu, G. Chen, Y. Wang, Y. Zhao, Versatile ice microneedles for transdermal delivery of diverse actives, Adv. Sci. 8 (17) (2021) 2101210.
[18] X.P. Zhang, B.L. Zhang, B.Z. Chen, Z.Q. Zhao, W.M. Fei, Y. Cui, X.D. Guo, Dissolving microneedle rollers for rapid transdermal drug delivery, Drug Deliv. Transl. Res. 12 (2) (2022) 459–471.
[19] F. Meng, A. Hasan, M. Mahdi Nejadi Babadaei, P. Hashemi Kani, A. Jouya Talaei, M. Sharifi, T. Cai, M. Falahati, Y. Cai, Polymeric-based microneedle arrays as potential platforms in the development of drugs delivery systems, J. Adv. Res. 26 (2020) 137–147.
[20] A.F. Moreira, C.F. Rodrigues, T.A. Jacinto, S.P. Miguel, E.C. Costa, I.J. Correia, Microneedle-based delivery devices for cancer therapy: a review, Pharmacol. Res. 148 (2019), 104438.
[21] B.Z. Chen, L.Q. Zhang, Y.Y. Xia, X.P. Zhang, X.D. Guo, A basal-bolus insulin regimen integrated microneedle patch for intraday postprandial glucose control, Sci. Adv. 6 (28) (2020) eaba7260.
[22] P. Yang, C. Lu, W. Qin, M. Chen, G. Quan, H. Liu, L. Wang, X. Bai, X. Pan, C. Wu, Construction of a core-shell microneedle system to achieve targeted co-delivery of checkpoint inhibitors for melanoma immunotherapy, Acta Biomater. 104 (2020) 147–157.
[23] S. Gorantla, U. Batra, E.R. Puppala, T. Waghule, V. Naidu, G. Singhvi, Emerging trends in microneedle-based drug delivery strategies for the treatment of rheumatoid arthritis, Expert Opin. Drug Deliv. 19 (4) (2022) 395–407.
[24] C. Wu, J. Cheng, W. Li, L. Yang, H. Dong, X. Zhang, Programmable polymeric microneedles for combined chemotherapy and antioxidative treatment of rheumatoid arthritis, ACS Appl. Mater. Interfaces 13 (46) (2021) 55559–55568.
[25] K. Yu, X. Yu, S. Cao, Y. Wang, Y. Zhai, F. Yang, X. Yang, Y. Lu, C. Wu, Y. Xu, Layered dissolving microneedles as a need-based delivery system to simultaneously alleviate skin and joint lesions in psoriatic arthritis, Acta Pharm. Sin. B 11 (2) (2021) 505–519.
[26] Q. Guo, X. Li, Y. Yang, J. Wei, Q. Zhao, F. Luo, Z. Qian, Enhanced 4T1 breast carcinoma anticancer activity by co-delivery of doxorubicin and curcumin with core–shell drug-carrier based on heparin modified poly(L-lactide) grafted polyethylenimine cationic nanoparticles, J. Biomed. Nanotechnol. 10 (2) (2014) 227–237.
[27] C. Richez, M. Truchetet, Evaluating filgotinib for the treatment of rheumatoid arthritis, Expert. Opin. Pharmacother. 22 (18) (2021) 2435–2444.
[28] S. Zhang, M. Zhang, X. Li, G. Li, B. Yang, X. Lu, Y. Gao, F. Sun, Nano-based co-delivery system for treatment of rheumatoid arthritis, Molecules 27 (18) (2022) 5973.
[29] Y. Li, S. Wei, Y. Sun, S. Zong, Y. Sui, Nanomedicine-based combination of dexamethasone palmitate and MCL-1 siRNA for synergistic therapeutic efficacy against rheumatoid arthritis, Drug Deliv. Transl. Res. 11 (6) (2021) 2520–2529.
[30] V.T. Francio, C. Towery, S. Davani, T.L. Brown, A clinical perspective of oral versus topical diclofenac sodium in the treatment of osteoarthritis, Arch. Phys. Med. Rehabil. 98 (10) (2017) e24–e25.
[31] Z. Ju, M. Li, J. Xu, D.C. Howell, Z. Li, F.E. Chen, Recent development on COX-2 inhibitors as promising anti-inflammatory agents: the past 10 years, Acta Pharm. Sin. B 12 (6) (2022) 2790–2807.
[32] P. Brooks, P. Kubler, Etoricoxib for arthritis and pain management, Ther. Clin. Risk Manag. 2 (1) (2006) 45–57.
[33] A. van Walsem, S. Pandhi, R.M. Nixon, P. Guyot, A. Karabis, R.A. Moore, Relative benefit-risk comparing diclofenac to other traditional non-steroidal anti-inflammatory drugs and cyclooxygenase-2 inhibitors in patients with osteoarthritis or rheumatoid arthritis: a network meta-analysis, Arthritis Res. Ther. 17 (1) (2015) 66.
[34] G. Affaitati, M.A. Giamberardino, D. Lapenna, R. Costantini, Diclofenac epolamine topical patch for the treatment of pain, J. Biol. Regul. Homeost. Agents 32 (3) (2018) 435–441.
[35] N. Ercan, M.O. Uludag, E.R. Agis, E. Demirel-Yilmaz, The anti-inflammatory effect of diclofenac is considerably augmented by topical capsaicinoids-containing patch in carrageenan-induced paw oedema of rat, Inflammopharmacology 21 (6) (2013) 413–419.
[36] D. Huang, M. Sun, Y. Bu, F. Luo, C. Lin, Z. Lin, Z. Weng, F. Yang, D. Wu, Microcapsule-embedded hydrogel patches for ultrasound responsive and enhanced transdermal delivery of diclofenac sodium, J. Mater. Chem. B 7 (14) (2019) 2330–2337.
[37] E. Proksch, J.M. Brandner, J. Jensen, The skin: an indispensable barrier, Exp. Dermatol. 17 (12) (2008) 1063–1072.
[38] G. Du, P. He, J. Zhao, C. He, M. Jiang, Z. Zhang, Z. Zhang, X. Sun, Polymeric microneedle-mediated transdermal delivery of melittin for rheumatoid arthritis treatment, J. Control. Release 336 (2021) 537–548.
[39] S. Nalamachu, J. Gudin, Characteristics of analgesic patch formulations, J. Pain Res. 13 (2020) 2343–2354.
[40] S. Lobo, S. Sachdeva, T. Goswami, Role of pressure-sensitive adhesives in transdermal drug delivery systems, Ther. Deliv. 7 (1) (2016) 33–48.
[41] M.A. Altamimi, S.H. Neau, Investigation of the in vitro performance difference of drug-Soluplus(R) and drug-PEG 6000 dispersions when prepared using spray drying or lyophilization, Saudi Pharm. J. 25 (3) (2017) 419–439.
[42] L. Zhang, Y. Li, F. Wei, H. Liu, Y. Wang, W. Zhao, Z. Dong, T. Ma, Q. Wang, Transdermal delivery of salmon calcitonin using a dissolving microneedle array: characterization, stability, and in vivo pharmacodynamics, AAPS PharmSciTech 22 (1) (2020) 1.
[43] Y. Li, X. Hu, Z. Dong, Y. Chen, W. Zhao, Y. Wang, L. Zhang, M. Chen, C. Wu, Q. Wang, Dissolving microneedle arrays with optimized needle geometry for transcutaneous immunization, Eur. J. Pharm. Sci. 151 (2020), 105361.
[44] X. Zhao, X. Li, P. Zhang, J. Du, Y. Wang, Tip-loaded fast-dissolving microneedle patches for photodynamic therapy of subcutaneous tumor, J. Control. Release 286 (2018) 201–209.
[45] J. Pan, W. Ruan, M. Qin, Y. Long, T. Wan, K. Yu, Y. Zhai, C. Wu, Y. Xu, Intradermal delivery of STAT3 siRNA to treat melanoma via dissolving microneedles, Sci. Rep. UK 8 (1) (2018) 1117.

[46] Y. Li, L. Zheng, W. Cao, X. Yang, Q. Wang, X. Gu, F. Liu, T. Ma, X. Wang, Q. Wang, 5-aminolevulinic acid-loaded dissolving microneedle array for photodynamic therapy of rheumatoid arthritis on rats, Biomed. Pharmacother. 162 (2023), 114684.

[47] M. Dul, M. Alali, M. Ameri, M.D. Burke, C.M. Craig, B.P. Creelman, L. Dick, R. F. Donnelly, M.N. Eakins, C. Frivold, A.H. Forster, P.A. Gilbert, S. Henke, S. Henry, D. Hunt, H. Lewis, H.I. Maibach, J.J. Mistilis, J.H. Park, M.R. Prausnitz, D. K. Robinson, C. Hernandez, C. Ross, J. Shin, T.J. Speaker, K.M. Taylor, D. Zehrung, J.C. Birchall, C. Jarrahian, S.A. Coulman, Assessing the risk of a clinically significant infection from a microneedle array patch (MAP) product, J. Control. Release 361 (2023) 236–245.

[48] C. Nastiti, Y. Mohammed, K.C. Telaprolu, X. Liang, J.E. Grice, M.S. Roberts, H. Benson, Evaluation of quantum dot skin penetration in porcine skin: effect of age and anatomical site of topical application, Skin Pharmacol. Physiol. 32 (4) (2019) 182–191.